JCTC Journal of Chemical Theory and Computation

pubs.acs.org/JCTC Article

Compensatory Mechanisms in Temperature Dependence of DNA Double Helical Structure: Bending and Elongation

Hana Dohnalová, Tomáš Dršata, Jiří Šponer, Martin Zacharias, Jan Lipfert,* and Filip Lankaš*

Cite This: https://dx.doi.org/10.1021/acs.jctc.0c00037 Read Online

ACCESS | Metrics & More | Article Recommendations | Supporting Information

ABSTRACT: Changes in the structure of double-stranded (ds) DNA with temperature affect processes in thermophilic organisms and are important for nanotechnological applications. Here we investigate temperature-dependent conformational changes of dsDNA at the scale of several helical turns and at the base pair step level, inferred from extensive all-atom molecular dynamics simulations of DNA at temperatures from 7 to 47 °C. Our results suggest that, contrary to twist, the overall bending of dsDNA without A-tracts depends only very weakly on temperature, due to the mutual compensation of directional local bends. Investigating DNA length as a function of temperature, we find that the sum of distances between base pair centers (the wire length) exhibits a large expansion coefficient of $\sim 2 \times 10^{-4}$ °C^{-1}, similar to values reported for thermoplastic materials. However, the wire length increase with temperature is absorbed by expanding helix radius, so the length measured along the helical axis (the spring length) seems to suggest a very small negative thermal expansion coefficient. These compensatory mechanisms contribute to thermal stability of DNA structure on the biologically relevant scale of tens of base pairs and longer.

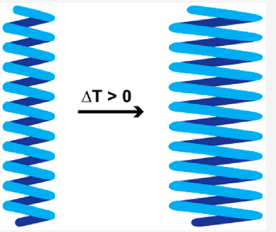

INTRODUCTION

Double-stranded DNA (dsDNA) serves as the repository of genetic information in all cellular life. It has to keep its integrity and biological function in the broad temperature range accessible to living organisms. To understand how this is achieved, one has to study how DNA properties such as its three-dimensional structure depend on temperature. Besides its biological relevance and general biophysical interest, temperature effects on DNA structure are also important in nanotechnological applications, helping to estimate thermal stability, temperature-dependent internal stresses, and structural changes of the supramolecular assemblies.

Most of the research on temperature dependence of double-stranded DNA structure so far has been focused on twist. In our recent work[1] (see also the literature survey therein), we reported magnetic tweezer experiments together with atomic-resolution, explicit solvent molecular dynamics (MD) simulations and coarse-grained simulations. The twist temperature dependence inferred from the atomistic MD was in quantitative agreement with the experimentally measured value of $-11.0 \pm 1.2°\cdot°C^{-1}\cdot kbp^{-1}$. Less is known about temperature dependence of other key DNA structural features, such as its contour length or equilibrium bending angle, which play a pivotal role in DNA interaction with proteins, nucleosome formation, and DNA packaging.

In the present work we investigate dsDNA bending and elongation as a function of temperature at two different length scales, based on extensive all-atom MD simulations. At the global scale of several helical turns, the molecule is described by means of global (or end-to-end) twist, global bending, and the molecule length, defined either along the curve connecting base pair centers (the wire length) or along the helical axis (the spring length). The observables at this global scale are directly related to what is probed in single-molecule optical and magnetic tweezer measurements.[2] The global effects result from contributions from the finer, local scale of individual base pair steps. We identify intrinsic compensatory mechanisms which reduce the temperature dependence of local bending and elongation to much smaller effects at the global scale.

METHODS

As the data source, we use our MD simulations reported earlier,[1] namely five microsecond-long unrestrained MD trajectories of a 33 base pair (bp) oligomer, each simulated at a different temperature (7, 17, 27, 37, and 47 °C). The oligomer sequence is mixed and does not contain A-tracts. The Amber OL15 force field[3] was used for the simulations. The sequence and the simulation protocol are detailed in the Supporting Information.

A researcher willing to perform MD simulations of duplex DNA using an Amber force field currently can make a choice between two state-of-the-art parameter sets, the bsc1[4] and the OL15.[3] Their performance has been thoroughly investigated by comparing multimicrosecond[5] and millisecond[6] benchmark simulations to experimental structural data. These studies concluded that any current research involving dsDNA

Received: January 14, 2020
Published: March 20, 2020

https://dx.doi.org/10.1021/acs.jctc.0c00037
J. Chem. Theory Comput. XXXX, XXX, XXX−XXX

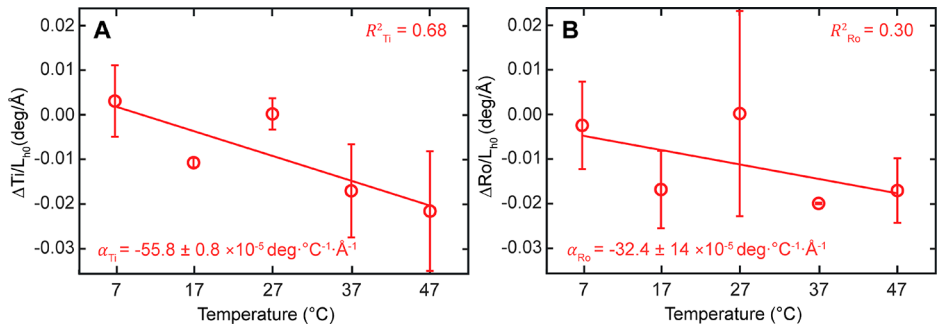

Figure 1. Temperature dependence of global tilt (Ti), the end-to-end bending angle toward the backbones at the oligomer center (A), and global roll (Ro), the bending angle toward the grooves at the same location (B). Only the tilt shows good linear dependence; the roll exhibits similar spread of values but with weak linear dependence. The thermal expansion coefficients are roughly an order of magnitude smaller than those of DNA twist. The index "0" denotes ensemble averages at the reference temperature T_0 = 27 °C.

simulations using Amber force fields should employ the bsc1 or OL15 modification,[6] and that both of them can be safely used to reproduce the structure of DNA duplexes, including sequence-dependent details.[5] Besides that, our recent work indicates that OL15 is able to quantitatively reproduce the temperature dependence of DNA twist.[1] This adds confidence to the use of OL15 in the present study.

To describe the global conformation, we define a frame at each end of the molecule by first averaging standard frames fixed to bases[7] in three pairs close to the end (pairs 2−4 and 30−32). The average frames are then projected onto the mean local helical axis of the three pairs[1] to obtain the end frames. Global (or end-to-end) rotational coordinates between the two end frames are defined in an exactly analogous manner as in the 3DNA conformational analysis algorithm.[8] In particular, global roll (denoted Ro) measures bending in the direction of the grooves at the oligomer center, while global tilt (Ti) describes bending toward the backbones at the same location. Besides that, we consider two different definitions of the double helix length. The first one, which we call the wire length and denote L, is the sum of distances d^a between the centers of base pairs a and $a + 1$, while the other, denoted L_h and called the spring length, is the sum of helical rises h^a, that is, the projections of d^a onto the local helical axis:

$$L = \sum_{a=1}^{N} d^a, \qquad L_h = \sum_{a=1}^{N} h^a \tag{1}$$

where N is the number of base pair steps involved (we start the numbering from 1 for simplicity). We measure the oligomer length between base pairs 3 and 31; thus N = 28. The local helical axis used here is the rotation axis of the screw transformation between base pairs a and $a + 1$.[8] We further define the centerline helix radius r^a as the perpendicular distance from the local helical axis to the center of base pair a (or the center of base pair $a + 1$—both distances are equal) and the helical twist ω^a as the rotation angle of the screw transformation. The definitions are illustrated in Figure S1. It will be useful to define the mean quantities r, h, d, and ω by the relations

$$r = \frac{1}{N}\sum_{a=1}^{N} r^a, \quad \omega = \frac{1}{N}\sum_{a=1}^{N} \omega^a, \quad d = L/N, \quad h = L_h/N \tag{2}$$

Ensemble averages at the reference temperature T_0 (T_0 = 27 °C) will be denoted by the index "0": L_0, L_{h0}, r_0, and so on. Base-fixed frames, local helical axes, base pair centers, and standard conformational descriptors (local base pair step and helical coordinates, backbone angles, etc.) are computed using 3DNA. Ensemble averages are approximated by the means taken over the MD trajectory at the given temperature. Errors are estimated by repeating the calculations for the first half and the second half of the trajectory and computing the mean difference with respect to the value for the whole trajectory. To indicate how well the linear dependence reproduces the observed data, we report the coefficient of determination R^2, equal to the square of the correlation coefficient.

RESULTS AND DISCUSSION

We start with the temperature dependence of the end-to-end bending. We quantified the global bending of the DNA helix in our simulations by computing the global roll (Ro) and global tilt (Ti) as described under Methods. Global tilt measures bending toward the backbones in the oligomer center, while global roll measures bending toward the grooves there. The results in Figure 1 show that the linear temperature dependence of DNA global tilt is rather well defined (R^2 = 0.68). Its slope, $(-55.8 \pm 0.8) \times 10^{-5}$°·°C^{-1}·Å^{-1}, is nearly an order of magnitude smaller than that of DNA end-to-end twist, reported earlier to be $(-342 \pm 9) \times 10^{-5}$°·°C^{-1}·Å^{-1}, or −11.1 ± 0.3°·°C^{-1}·kbp^{-1}.[1] The DNA global roll displays a similar spread of values as the global tilt but with weak linear dependence (R^2 = 0.30).

Thus, the temperature dependence of DNA end-to-end bending is much weaker than that of end-to-end twist. The origin of this finding can be understood by looking at the temperature dependencies of the local base pair step coordinates (Figure S2). At the local level, the sequence averaged temperature change of roll is comparable to that of twist, while tilt changes much less. This means that the temperature change of local bending proceeds mostly via roll and is on average about as large as the change of local twist. The roll temperature slope is positive, meaning that roll increases with temperature; i.e., the increase of local bending is directed toward the major groove. However, while local twists accumulate along the DNA and largely determine the temperature dependence of end-to-end twist (Figure S3), bending via roll takes place in different directions (globally seen) due to the helical structure of the molecule. The local bends therefore tend to cancel each other, resulting only in a

https://dx.doi.org/10.1021/acs.jctc.0c00037
J. Chem. Theory Comput. XXXX, XXX, XXX−XXX

very small change of the global bending. This provides a compensatory mechanism that reduces the effect of temperature-dependent local bends on the overall bending of the DNA double helix.

The bending of DNA influences its superhelical state, the formation of regulatory loops, and binding to proteins. Our results suggest that changes in temperature affect permanent bending of DNA (devoid of A-tracts) at the scale of several helical turns by a negligible amount. Thus, temperature effects on bending would probably be dominated by changes in DNA persistence length, which decreases with temperature.[9−11]

The near temperature neutrality of global DNA bending predicted by our simulations may not apply to DNA molecules containing A-tracts, sequences of several adenines or thymines without a TA base pair step.[12] A-tracts induce bending of the DNA helix due to their particular structure, although the bending magnitude strongly depends on the ionic conditions.[13] If phased with the DNA helical repeat, their bending contributions add up and may result in a substantial global bend. However, at elevated temperatures (but still below the melting temperature), A-tracts undergo a structural change known as premelting[14,15] and their bending capacity is lost. This causes straightening of a DNA molecule containing phased A-tracts at higher temperatures. Polypurine tracts are also important in the context of DNA·RNA hybrids where the asymmetry in the purine content between the DNA and RNA strands has profound biological implications, as reported in a recent extensive study.[16]

Another important quantity is the molecule length. An idealized dsDNA adopts the canonical B-form, with the base pair centers lying on a straight helical axis. In real dsDNA, the base pair centers are somewhat displaced from the axis. One can imagine such a DNA molecule as a spring made of a wire connecting the base pair centers. Assume first that the spring is perfectly regular and straight. The spring length measured along the axis is L_h, the sum of helical rises (eq 1 and Figure S1). A simple calculation (see the Supporting Information) shows that the cosine of the angle between the helix tangent vector and the helical axis is equal to the ratio between the helical axis length and the helix contour length. The contour length is approximately equal to the sum of base pair center distances L (the wire length, eq 1). Therefore, we define the angle β by the relation

$$\cos \beta = L_h/L \tag{3}$$

and call it the molecule helicity (other closely related terms are "springiness"[17] and "crookedness"[18]). Real DNA molecules deviate from the perfectly straight regular spring, showing some degree of heterogeneity due to sequence-specific structural variations. However, a local helical axis between two adjacent pairs can still be defined as the rotation axis of the screw transformation connecting these pairs (see Methods). We introduce the local helicity β^a between pairs a and $a + 1$ by the ratio between the helical rise h^a and the base pair center distance d^a:

$$\cos \beta^a = h^a/d^a \tag{4}$$

It has long been understood that DNA helicity must be taken into account to properly map local base pair step shape and stiffness onto the wormlike chain level of description.[19] The dsDNA stretching deformation, i.e., increase of the spring length by applied force, seems to proceed largely by decreasing its helicity while the base pair distances change only weakly.[18,20]

The ensemble averaged values of the helix geometrical parameters are listed in Table 1. The local radii r^a and helicities β^a (Figure S4), despite some heterogeneity, are fully consistent with these results. The mean helical rise is comparable to the crystallographic, sequence averaged B-form value of 3.29 Å[7] as well as to the experimental value in solution, measured to be 3.27 ± 0.1 Å using SAXS with gold labels[21] and 3.23 ± 0.1 Å using anomalous SAXS with gold labels.[22] The mean helical twist is roughly halfway between the crystallographic value of 36.5°[7] and 34.3°, the predicted solution twist computed for our sequence using dinucleotide step values from cyclization experiments (Table S2 of ref 23). The values for the individual steps (Figure S5) again indicate only moderate heterogeneity of the helix.

Table 1. Geometrical Parameters of the dsDNA Helix Studied in This Work at the Reference Temperature T_0 = 27 °C[a]

wire length (Å)	L_0	97.96 ± 0.02
spring length (Å)	L_{h0}	90.77 ± 0.05
helicity (deg)	β_0	21.98 ± 0.04
mean radius (Å)	r_0	1.98 ± 0.00
mean helical twist (deg)	ω_0	35.60 ± 0.01
mean helical rise (Å)	h_0	3.24 ± 0.00
mean base pair center distance (Å)	d_0	3.50 ± 0.00

[a]The values and errors are computed as described under Methods.

How does the wire length L change with temperature, and how is it related to the change of the spring length L_h? As a simple model, one can imagine a pure elongation of the wire with constant helicity (eq 3), in which case the relative changes of L and L_h would be the same. However, this is not at all what the data show.

Figure 2 displays relative changes of ensemble averaged L and L_h with temperature. The change in wire length L closely follows a linear dependence, with the linear expansion coefficient of $(221 \pm 2) \times 10^{-6}$ °C^{-1}. The value is close to the upper limit of reported linear expansion coefficients for most of the thermoplastic materials (https://passive-components.eu/). The thermal change of the wire length is dominated by the change of accumulated local rises (Figure S2).

In contrast, the spring length L_h behaves very differently—its thermal change is very weak compared to that of the wire length L (Figure 2). The data seem to suggest a very slight decrease of L_h with temperature, but the linear fit is so poor (R^2 = 0.27) that we cannot make any well-founded conclusion as to the exact magnitude or the sign of the thermal expansion coefficient.

The observed elongation of the DNA wire thus does not transform into the change of its spring length and must be absorbed somewhere else. To investigate this point, we express the base pair center distance d^a of step a as a function of the centerline helix radius r^a, the helical rise h^a, and the helical twist ω^a as defined under Methods and in Figure S1. We write

$$d^a = f(r^a, h^a, \omega^a) \tag{5}$$

and from the definitions (see Figure S1) we deduce that

$$f(r^a, h^a, \omega^a) = \sqrt{(h^a)^2 + 2(r^a)^2(1 - \cos \omega^a)} \tag{6}$$

https://dx.doi.org/10.1021/acs.jctc.0c00037
J. Chem. Theory Comput. XXXX, XXX, XXX−XXX

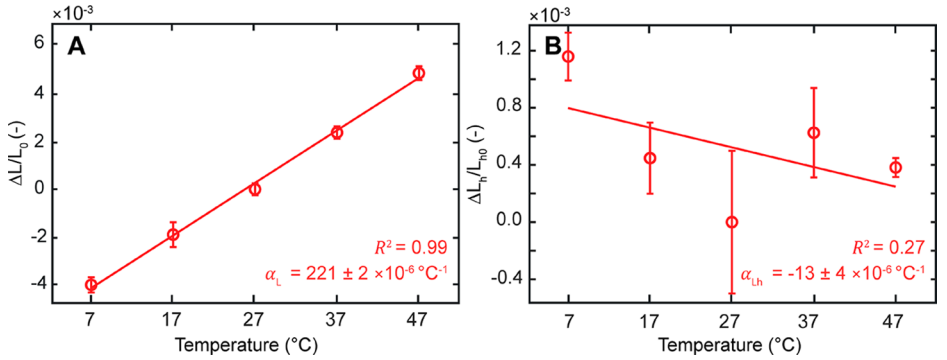

Figure 2. Relative elongation of the DNA duplex. The wire length L (A) is defined as the sum of distances between successive base pair centers. It expands linearly with temperature, the expansion coefficient being within the range reported for thermoplastic materials. In contrast, the spring length L_h (B), measured along the helical axis, changes much less with temperature. Its thermal expansion coefficient is negative, but the linear dependence is very weak.

In this way the wire length L (the sum of d^a, eq 1) is expressed as a function of r^a, h^a, and ω^a of the individual steps. Taking the ensemble averages at temperature T and at the reference temperature T_0 (T_0 = 27 °C), we find, to the approximation detailed in the Supporting Information (eq B19) and verified in Figure S6, that

$$\langle L\rangle_T - \langle L\rangle_{T_0} = \sum_{a=1}^{N} [f(\langle r^a\rangle_T, \langle h^a\rangle_T, \langle \omega^a\rangle_T) - f(\langle r^a\rangle_{T_0}, \langle h^a\rangle_{T_0}, \langle \omega^a\rangle_{T_0})] \quad (7)$$

Equations 6 and 7 enable us to study the effect of thermal changes of r^a, h^a, and ω^a on L separately. Changing in eq 7 the radii $\langle r^a\rangle_T$ alone while keeping the other variables constant (at their T_0 ensemble averaged values) explains almost all of the temperature increase in $\langle L\rangle_T$, while temperature changes of $\langle h^a\rangle_T$ and $\langle \omega^a\rangle_T$ have nearly no effect (Figure S7). Thus, the thermal increase of the wire length is primarily associated with the increase of the helical radius, while it only very weakly depends on the thermal changes of helical rise and helical twist. This enables us to express the thermal expansion coefficient of the radius as a function of the thermal expansion coefficient of the wire length. To this end we replace in eq 7 the sequence-specific, temperature-dependent quantities $\langle h^a\rangle_T$ and $\langle \omega^a\rangle_T$ by their sequence averaged values at T_0, that is, h_0 and ω_0 (Table 1). We also neglect the heterogeneity of the radius and approximate all $\langle r^a\rangle_T$ by their sequence average $\langle r\rangle_T$ (eq 2). Taking the temperature derivative of both sides of eq 7, evaluating it at T_0, and summing over all a, we deduce that

$$\left(\frac{d\langle r\rangle_T}{dT}\right)_{T=T_0} = \frac{d_0}{b_0}\left(\frac{1}{L_0}\frac{d\langle L\rangle_T}{dT}\right)_{T=T_0} \quad (8)$$

where

$$b_0 = \frac{2(1-\cos\omega_0)}{\sqrt{(h_0/r_0)^2 + 2(1-\cos\omega_0)}} \quad (9)$$

Substituting the thermal expansion coefficient of L (Figure 2) into the right-hand side of eq 8, we obtain an estimate of the thermal expansion coefficients of r. The estimated value is similar to the value inferred directly from the MD data (Figure 3).

The near temperature independence of L_h enables us to estimate the thermal change of the helicity β as well. We

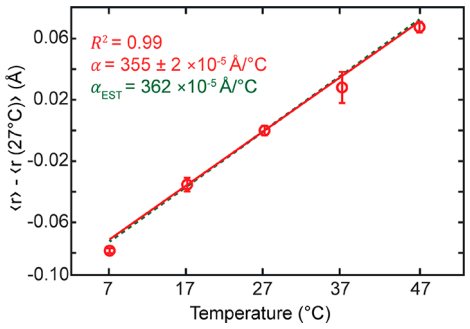

Figure 3. Temperature change of sequence averaged radius r of the centerline helix (eq 2). The slope estimated from eqs 8 and 9, α_{EST}, is close to the slope α inferred directly from the MD simulations.

substitute L_{h0} for L_h in eq 3 and write $\beta = \arccos(L_{h0}/L)$, and then we take the ensemble average, make use of the approximation of eq B19 in the Supporting Information, and compute the derivative with respect to T. We obtain

$$\left(\frac{d\langle\beta\rangle_T}{dT}\right)_{T=T_0} = \frac{1}{\sqrt{(L_0/L_{h0})^2 - 1}}\left(\frac{1}{L_0}\frac{d\langle L\rangle_T}{dT}\right)_{T=T_0} \quad (10)$$

The insertion of the thermal expansion coefficient for L (Figure 2) yields the thermal slope of the helicity close to the one actually observed in the MD data (Figure 4).

Thus, the thermal expansion of the DNA wire length is associated with the expansion of the centerline helix radius and the increase of helicity, while the length measured along the

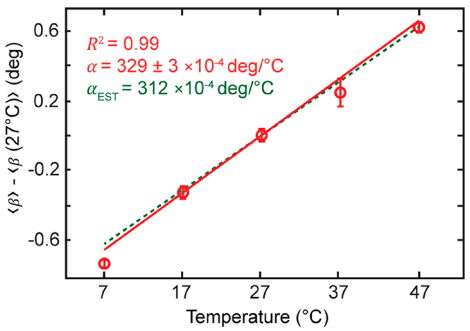

Figure 4. Temperature change of the helicity β (eq 3). The slope estimated from eq 10 is similar to the value inferred directly from the MD data.

https://dx.doi.org/10.1021/acs.jctc.0c00037
J. Chem. Theory Comput. XXXX, XXX, XXX−XXX

helical axis (spring length) stays nearly constant. This compensatory mechanism, summarized in Figure 5, ensures

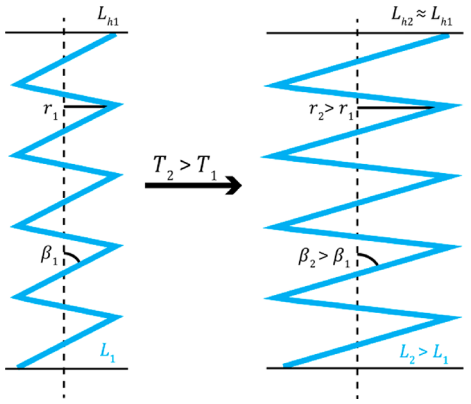

Figure 5. Compensatory mechanism ensuring near temperature neutrality of dsDNA length measured along the helical axis (spring length, L_h). The increase in the sum of distances between adjacent base pair centers (wire length, L) is absorbed into the increased radius of the centerline helix r and increased helicity β, while the spring length stays nearly constant.

that thermally induced changes of the base pair center distances have a minimal effect on the overall length of the DNA double helix. Notice that the thermal elongation is proportional to the molecule length; thus if this was a major effect, it might be detrimental for the spatial positioning of the ends of long DNA molecules. In contrast, the temperature increase of the radius is independent of the molecule length.

What is the microscopic mechanism of the observed temperature dependence? The DNA helix is stable in our simulations, save for the fraying of end base pairs and rare, short-lived inner hydrogen bond breaks (Figure S8). To see how these internal breaks affect the temperature dependence of DNA structure, we filtered out all the MD snapshots where at least one hydrogen bond in any pair except terminal ones was broken (the cutoff distance was 4 Å between heavy atoms) and repeated our analysis on the remaining snapshots with intact base pairing. Both global and local temperature dependencies changed only slightly; thus the loss of base pairing is not the dominant mechanism. Another possible candidate is the dynamics of backbone torsion angles (Figures S9 and S10). The DNA backbone undergoes rare and short-lived flips of the torsion angles α and γ to noncanonical values (α/γ in $g+/t$ rather than the canonical $g-/g+$); besides that, we observe yet another, even more rare noncanonical state where $\alpha/\varepsilon/\zeta$ are in $t/g+/g+$. Again, filtering out snapshots with at least one of these flips anywhere except terminal steps changes the observed temperature dependencies by a negligible amount. In contrast to these rare states, the DNA backbone frequently switches back and forth between the BI (ε/ζ in $t/g-$) and BII (ε/ζ in $g-/t$) states (Figure S10).[24−28] It has been suggested that local twist, and possibly also the other local coordinates, depend on the BI/BII state of the backbone fragments within the given step as well as in the nearest neighboring steps on the 3′ side[25,26] and 5′ side.[28] To isolate the effect of BI/BII, we recomputed the local temperature dependencies of each step using only the snapshots where the backbone in that step and its 5′ and 3′ nearest neighbors were all in the BI state (Figure S11). Although the temperature response of some steps changed, the sequence averaged values differ only slightly from those for the whole, unfiltered trajectory (compare Figure S11 to Figure S2). Thus, our data suggest that the temperature dependence of sequence averaged DNA local structure is not determined by the BI/BII backbone dynamics. Finally, the glycosidic angles χ and the sugar puckers all stay within their canonical *anti* and C2′-*endo* domains, respectively, with systematically lower pucker values of pyrimidines (Figure S12A). While the temperature dependencies of the individual puckers are quite heterogeneous (Figure S12B), the sequence averaged sugar pucker clearly decreases with temperature (Figure 6).

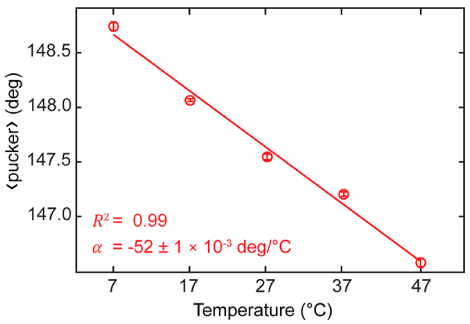

Figure 6. Temperature dependence of the mean sugar pucker.

These findings indicate that the observed temperature dependence of DNA structure cannot be explained by thermally induced structural anomalies. Rather, we have to turn to the properties of the double helix itself. As detailed in the Supporting Information, the helical rise h^a of step a can be, in a certain approximation, estimated as

$$h^a_{\mathrm{EST}} = d^a - \frac{d^a}{2}\left(\frac{\Gamma^a}{\Omega^a}\right)^2 \tag{11}$$

where d^a is the base pair center distance, Γ^a is the local bending angle, and Ω^a is the local twist of step a. Summing over all the steps (see eq 1) and taking the ensemble average at temperature T, we obtain

$$\langle L_{h,\mathrm{EST}}\rangle_T = \langle L\rangle_T - \left\langle \sum_{a=1}^{N} \frac{d^a}{2}\left(\frac{\Gamma^a}{\Omega^a}\right)^2 \right\rangle_T \tag{12}$$

Thus, the temperature dependence of the spring length (left-hand side of eq 12) can be estimated as the difference between the temperature change of the wire length (first term on the right-hand side) and that of another term depending on the local bending and twisting. As before, we replace the ensemble averages by MD trajectory averages and perform a least-squares linear fit of the values for the five temperatures. The temperature dependence of L is characterized by the expansion coefficient $\alpha_L = 221 \times 10^{-6}$ °C^{-1} (see Figure 2A). This expansion, however, is almost fully compensated by the second term on the right-hand side of eq 12, resulting in the estimated thermal expansion of the spring length $\alpha_{L_{h,\mathrm{EST}}} = -10 \times 10^{-6}$ °C^{-1}, an order of magnitude lower than α_L and close to $\alpha_{L_h} = -13 \times 10^{-6}$ °C^{-1} inferred directly from the MD data (Figure 2B). Thus, the near temperature neutrality of the DNA spring length is due to the compensation of the base pair center distance expansion by another thermal change involving local bending and twisting.

https://dx.doi.org/10.1021/acs.jctc.0c00037
J. Chem. Theory Comput. XXXX, XXX, XXX−XXX

The temperature response of DNA structure is expected to depend on the sequence, even in the absence of A-tracts. To study the sequence dependence exhaustively, one would have to examine the full set of sequences at least 10 bp long, since it is at the scale of one helical turn that the local thermally induced bends via roll cancel out. This is impossible to do by means of atomistic molecular dynamics. To get some insight into the sequence dependence, we repeated the computations for a sliding window of 10 base pairs shifted in 1 bp steps along the oligomer. While the GC content in the whole oligomer is 52%, the values for the sequence windows vary between 40 and 70% (Figure S13). All the thermal expansion coefficients, with the exception of α_{L_h} (spring length), deviate by at most 20% from the full oligomer values (Figure S14). The spring length coefficient, in contrast, varies as much as 4-fold, although it is still at least 3 times lower than the wire length expansion coefficient α_L. At the scale of ∼30 base pairs (the whole oligomer), sequence-dependent variations of α_{L_h} are further averaged out to achieve a value an order of magnitude smaller than α_L (Figure 2). None of the expansion coefficients is correlated with the GC content ($R^2 < 0.05$).

Finally, we look at the convergence of our results. Repeating the computation for the whole oligomer using a 200 ns sliding window shifted in 10 ns steps (Figure S15), we observe substantial deviations of the expansion coefficients from the full trajectory values (severalfold for α_{L_h} and 20−30% for the rest). The wavelike character of the deviations (Figure S15) may reflect slow, large-scale thermally induced motions of the oligomer and suggests that simulations much shorter than 1 μs would give unreliable results.

CONCLUSIONS

Understanding biological processes in thermophilic organisms or thermal effects in DNA nanostructures requires information about the temperature dependence of double-stranded DNA structure. Here we tackle this problem using extensive all-atom molecular dynamics (MD) simulations of a DNA helix devoid of A-tracts at different temperatures and MD data analysis at the length scale of several helical turns as well as at the local base pair step level. We identify compensatory mechanisms by which local temperature-induced structural changes are eliminated at the longer scale: changes in local bends are directional and are canceled due to the DNA helical structure, while the increased contour length of the helix connecting base pair centers is absorbed into the increased helical radius. The sequence averaged local thermal changes are not associated with the conformational transitions between BI and BII backbone substates.

ASSOCIATED CONTENT

Supporting Information

The Supporting Information is available free of charge at https://pubs.acs.org/doi/10.1021/acs.jctc.0c00037.

Supplementary theory, methods, and figures (PDF)

AUTHOR INFORMATION

Corresponding Authors

Filip Lankaš − *Department of Informatics and Chemistry, University of Chemistry and Technology Prague, 166 28 Prague, Czech Republic*; Email: filip.lankas@vscht.cz

Jan Lipfert − *Department of Physics and Center for Nanoscience, LMU Munich, 80799 Munich, Germany*; orcid.org/0000-0003-3613-7896; Email: Jan.Lipfert@lmu.de

Authors

Hana Dohnalová − *Department of Informatics and Chemistry, University of Chemistry and Technology Prague, 166 28 Prague, Czech Republic*

Tomáš Dršata − *Department of Informatics and Chemistry, University of Chemistry and Technology Prague, 166 28 Prague, Czech Republic; Institute of Biophysics of the Czech Academy of Sciences, 612 65 Brno, Czech Republic*

Jiří Šponer − *Institute of Biophysics of the Czech Academy of Sciences, 612 65 Brno, Czech Republic*; orcid.org/0000-0001-6558-6186

Martin Zacharias − *Physics-Department T38, Technical University of Munich, 85748 Garching, Germany*; orcid.org/0000-0001-5163-2663

Complete contact information is available at: https://pubs.acs.org/10.1021/acs.jctc.0c00037

Notes

The authors declare no competing financial interest.

ACKNOWLEDGMENTS

The Grant Agency of the Czech Republic [17-14683S to H.D., T.D., and F.L.], the German Research Foundation (DFG) through Sonderforschungsbereich [SFB 863, Projects A10 and A11 to J.L. and M.Z.], and ERDF [Project SYMBIT, Reg. No. CZ.02.1.01/0.0/0.0/15_003/0000477 to J.S.] are acknowledged.

REFERENCES

(1) Kriegel, F.; Matek, C.; Drsata, T.; Kulenkampff, K.; Tschirpke, S.; Zacharias, M.; Lankas, F.; Lipfert, J. The temperature dependence of the helical twist of DNA. *Nucleic Acids Res.* **2018**, *46*, 7998−8009.

(2) Kriegel, F.; Ermann, N.; Lipfert, J. Probing the mechanical properties, conformational changes, and interactions of nucleic acids with magnetic tweezers. *J. Struct. Biol.* **2017**, *197*, 26−36.

(3) Zgarbova, M.; Sponer, J.; Otyepka, M.; Cheatham III, T. E.; Galindo-Murillo, R.; Jurecka, P. Refinement of the sugar-phosphate backbone torsion beta for Amber force fields improves the description of Z- and B-DNA. *J. Chem. Theory Comput.* **2015**, *11*, 5723−5736.

(4) Ivani, I.; Dans, P. D.; Noy, A.; Perez, A.; Faustino, I.; Hospital, A.; Walther, J.; Andrio, P.; Goni, R.; Balaceanu, A.; Portella, G.; Battistini, F.; Gelpi, J. L.; Gonzalez, C.; Vendruscolo, M.; Laughton, C. A.; Harris, S. A.; Case, D. A.; Orozco, M. Parmbsc1: a refined force field for DNA simulations. *Nat. Methods* **2016**, *13*, 55−58.

(5) Dans, P. D.; Ivani, I.; Hospital, A.; Portella, G.; Gonzalez, C.; Orozco, M. How accurate are accurate force-fields for B-DNA? *Nucleic Acids Res.* **2017**, *45*, 4217−4230.

(6) Galindo-Murillo, R.; Robertson, J. C.; Zgarbova, M.; Sponer, J.; Otyepka, M.; Jurecka, P.; Cheatham III, T. E. Assessing the current state of Amber force field modifications for DNA. *J. Chem. Theory Comput.* **2016**, *12*, 4114−4127.

(7) Olson, W. K.; Bansal, M.; Burley, S. K.; Dickerson, R. E.; Gerstein, M.; Harvey, S. C.; Heinemann, U.; Lu, X.-J.; Neidle, S.; Shakked, Z.; Sklenar, H.; Suzuki, M.; Tung, C.-S.; Westhof, E.; Wolberger, C.; Berman, H. M. A standard reference frame for the description of nucleic acid base-pair geometry. *J. Mol. Biol.* **2001**, *313*, 229−237.

(8) Lu, X.-J.; Olson, W. K. 3DNA: a software package for the analysis, rebuilding and visualization of three-dimensional nucleic acid structures. *Nucleic Acids Res.* **2003**, *31*, 5108−5121.

(9) Geggier, S.; Kotlyar, A.; Vologodskii, A. Temperature dependence of DNA persistence length. *Nucleic Acids Res.* **2011**, *39*, 1419−1426.
(10) Driessen, R. P. C.; Sitters, G.; Laurens, N.; Moolenaar, G. F.; Wuite, G. J. L.; Goosen, N.; Dame, R. T. Effect of temperature on the intrinsic flexibility of DNA and its interaction with architectural proteins. *Biochemistry* **2014**, *53*, 6430−6438.
(11) Schurr, J. M. Temperature-dependence of the bending elastic constant of DNA and extension of the two-state model. Tests and new insights. *Biophys. Chem.* **2019**, *251*, 106146.
(12) Haran, T. E.; Mohanty, U. The unique structure of A-tracts and intrinsic DNA bending. *Q. Rev. Biophys.* **2009**, *42*, 41−81.
(13) Stellwagen, E.; Peters, J. P.; Maher III, L. J.; Stellwagen, N. C. DNA A-tracts are not curved in solutions containing high concentrations of monovalent cations. *Biochemistry* **2013**, *52*, 4138−4148.
(14) Herrera, J. E.; Chaires, J. B. A premelting conformational transition in poly(dA)-poly(dT) coupled to daunomycin binding. *Biochemistry* **1989**, *28*, 1993−2000.
(15) Chan, S. S.; Breslauer, K. J.; Hogan, M. E.; Kessler, D. J.; Austin, R. H.; Ojemann, J.; Passner, J. M.; Wiles, N. C. Physical studies of DNA premelting equilibria in duplex with and without homo dA-dT tracts: correlations with DNA bending. *Biochemistry* **1990**, *29*, 6161−6171.
(16) Terrazas, M.; Genna, V.; Portella, G.; Villegas, N.; Sanchez, D.; Arnan, C.; Pulido-Quetglas, C.; Johnson, R.; Guigo, R.; Brun-Heath, I.; Avino, A.; Eritja, R.; Orozco, M. The origins and the biological consequences of the Pur/Pyr DNA.RNA asymmetry. *Chem.* **2019**, *5*, 1619−1631.
(17) Lipfert, J.; Skinner, G. M.; Keegstra, J. M.; Hensgens, T.; Jager, T.; Dulin, D.; Kober, M.; Yu, Z.; Donkers, S. P.; Chou, F. C.; Das, R.; Dekker, N. H. Double-stranded RNA under force and torque: Similarities to and striking differences from double-stranded DNA. *Proc. Natl. Acad. Sci. U. S. A.* **2014**, *111*, 15408−15413.
(18) Marin-Gonzalez, A.; Vilhena, J. G.; Moreno-Herrero, F.; Perez, R. DNA crookedness regulates DNA mechanical properties at short length scales. *Phys. Rev. Lett.* **2019**, *122*, 048102.
(19) Becker, N.; Everaers, R. From rigid base pairs to semiflexible polymers: Coarse-graining DNA. *Phys. Rev. E* **2007**, *76*, 021923.
(20) Marin-Gonzalez, A.; Vilhena, J. G.; Perez, R.; Moreno-Herrero, F. Understanding the mechanical response of double-stranded DNA and RNA under constant stretching force using all-atom molecular dynamics. *Proc. Natl. Acad. Sci. U. S. A.* **2017**, *114*, 7049−7054.
(21) Mathew-Fenn, R. S.; Das, R.; Harbury, P. A. Remeasuring the double helix. *Science* **2008**, *322*, 446−449.
(22) Zettl, T.; Mathew, R. S.; Seifert, S.; Doniach, S.; Harbury, P. A.; Lipfert, J. Absolute Intramolecular Distance Measurements with Angstrom-Resolution Using Anomalous Small-Angle X-ray Scattering. *Nano Lett.* **2016**, *16*, 5353−5357.
(23) Geggier, S.; Vologodskii, A. Sequence dependence of DNA bending rigidity. *Proc. Natl. Acad. Sci. U. S. A.* **2010**, *107*, 15421−15426.
(24) Heddi, B.; Oguey, C.; Lavelle, C.; Foloppe, N.; Hartmann, B. Intrinsic flexibility of B-DNA: the experimental TRX scale. *Nucleic Acids Res.* **2010**, *38*, 1034−1047.
(25) Drsata, T.; Perez, A.; Orozco, M.; Morozov, A. V.; Sponer, J.; Lankas, F. Structure, stiffness and substates of the Dickerson-Drew dodecamer. *J. Chem. Theory Comput.* **2013**, *9*, 707−721.
(26) Pasi, M.; Maddocks, J. H.; Beveridge, D. L.; Bishop, T. C.; Case, D. A.; Cheatham III, T. E.; Dans, P. D.; Jayaram, B.; Lankas, F.; Laughton, C. A.; Mitchell, J.; Osman, R.; Orozco, M.; Perez, A.; Petkeviciute, D.; Spackova, N.; Sponer, J.; Zakrzewska, K.; Lavery, R. *μ*ABC: a systematic microsecond molecular dynamics study of tetranucleotide sequence effects in B-DNA. *Nucleic Acids Res.* **2014**, *42*, 12272−12283.
(27) Dans, P. D.; Faustino, I.; Battistini, F.; Zakrzewska, K.; Lavery, R.; Orozco, M. Unraveling the sequence-dependent polymorphic behavior of d(CpG) steps in B-DNA. *Nucleic Acids Res.* **2014**, *42*, 11304−11320.
(28) Zgarbova, M.; Jurecka, P.; Lankas, F.; Cheatham III, T. E.; Sponer, J.; Otyepka, M. Influence of BII backbone substates on DNA twist: A unified view and comparison of simulation and experiment for all 136 distinct tetranucleotide sequences. *J. Chem. Inf. Model.* **2017**, *57*, 275−287.

https://dx.doi.org/10.1021/acs.jctc.0c00037
J. Chem. Theory Comput. XXXX, XXX, XXX−XXX